MANCHESTER
1824
The University of Manchester

SiGe-on-insulator fabricated via germanium condensation following high-fluence Ge+ ion implantation

DOI:
10.1063/1.4998457

Document Version
Accepted author manuscript

Link to publication record in Manchester Research Explorer

Citation for published version (APA):
Anthony, R., Haddara, Y. M., Crowe, I., & Knights, A. P. (2017). SiGe-on-insulator fabricated via germanium condensation following high-fluence Ge+ ion implantation. *Journal of Applied Physics*, *122*, [065306]. https://doi.org/10.1063/1.4998457

Published in:
Journal of Applied Physics

Citing this paper
Please note that where the full-text provided on Manchester Research Explorer is the Author Accepted Manuscript or Proof version this may differ from the final Published version. If citing, it is advised that you check and use the publisher's definitive version.

General rights
Copyright and moral rights for the publications made accessible in the Research Explorer are retained by the authors and/or other copyright owners and it is a condition of accessing publications that users recognise and abide by the legal requirements associated with these rights.

Takedown policy
If you believe that this document breaches copyright please refer to the University of Manchester's Takedown Procedures [http://man.ac.uk/04Y6Bo] or contact uml.scholarlycommunications@manchester.ac.uk providing relevant details, so we can investigate your claim.

Download date:22. Nov. 2022

SiGe-On-Insulator Fabricated via Germanium Condensation following High-Fluence Ge^+ Ion Implantation

R. Anthony,[1] Y. M. Haddara,[2] I. F. Crowe[3], and A. P. Knights*[1]

[1]*Department of Engineering Physics, McMaster University, Hamilton, L8S 4L7, Canada*

[2]*Department of Electrical and Computer Engineering, McMaster University, Hamilton, L8S 4K1, Canada*

[3]*School of Electrical and Electronic Engineering and the Photon Science Institute, The University of Manchester, M13 9PL, United Kingdom*

**contact author aknight@mcmaster.ca*

ABSTRACT

Germanium condensation is demonstrated using a two-step wet oxidation of germanium implanted Silicon-On-Insulator (SOI). Samples of 220nm thick SOI are implanted with a nominal fluence of $5x10^{16}cm^{-2}$ Ge^+ at an energy of 33keV. Primary post-implantation wet oxidation is performed initially at 870°C for 70 minutes, with the aim of capping the sample without causing significant dose loss via Ge evaporation through the sample surface. This is followed by a secondary higher temperature wet oxidation at either 900°C, 1000°C or 1080°C. The germanium retained dose and concentration profile, and the oxide thickness is examined after primary oxidation, and various secondary oxidation times, using Rutherford backscattering analysis. A mixed SiGe oxide is observed to form during the primary oxidation followed by a pure silicon oxide after higher temperature secondary oxidation. The peak germanium concentration, which varies with secondary oxidation condition, is found to range from 43 at- %

to 95 at- %, while the FWHM of the Ge profile varies from 13 to 5 nm, respectively. It is also observed that both the diffusion of germanium and the rate of oxidation are enhanced at 870°C and 900°C compared to equilibrium expectations. Transmission electron microscopy of a representative sample with secondary oxidation at 1080°C for 20 minutes shows that the SiGe layer is crystalline in nature and seeded from the underlying silicon. Raman spectroscopy is used to determine residual strain in the SiGe region following secondary oxidation. The strain is compressive in nature and increases with Ge concentration to a maximum of approximately 1% in the samples probed. In order to elucidate the physical mechanisms, which govern the implantation-condensation process, we fit the experimental profiles of the samples with a model that uses a modified segregation boundary condition; a modified linear rate constant for the oxidation; and an enhanced diffusion coefficient of germanium where the enhancement is inversely proportional to the temperature and decays with increasing time. Comparison of the modeled and experimental results shows reasonable agreement and allows conclusions to be made regarding the dominant physical mechanisms, despite the semi-empirical nature of the model used.

I. INTRODUCTION

Research on germanium (Ge) and silicon-germanium (SiGe) thin films has reemerged as a topic of considerable interest in optoelectronics and microelectronics. For microelectronics, Ge-based thin films offer higher electron and hole mobility compared to silicon that can be further increased via strain engineering. Such materials are likely to be of interest for fabrication of fully depleted MOSFETs and as Silicon-On-Insulator-Germanium-On-Insulator (SOI–GeOI) hybrid substrates for planar co-integration at the microprocessor or transistor levels [1]. In silicon-based optoelectronics Ge is commonly used as a process compatible detector material [2-5], and has

been demonstrated to exhibit lasing, albeit with a large threshold current and relatively poor slope efficiency [6]. Ge and SiGe can also be fabricated in a thin film form on silicon for applications which include waveguide formation for extended wavelengths [7].

An elegant method for the formation of high-Ge content Si_xGe_{1-x}-On-Insulator (here arbitrarily defined as $x<0.15$) is the so-called germanium condensation technique in which low-Ge content silicon-germanium (for example $x>0.9$) is epitaxially grown on Silicon-On-Insulator (SOI) and then thermally oxidized [8]. Under appropriate conditions, Si is oxidized preferentially over the Ge while the growing oxide layer and buried oxide layer act as a diffusion barrier resulting in the growth of a thin layer of high-Ge content, epitaxial SiGe. Whereas in reference [8] (for example), Ge was introduced via an epitaxial growth process, there has been some work investigating Ge condensation whereby the Ge is introduced via high-fluence ion implantation. The significant difference being that the implanted volume is amorphous in nature and relies on seeding from the single-crystal silicon below to create a crystalline SiGe layer during oxidation. Previous results show that the preferential oxidation of Si and pile-up of Ge at the interface occurs for both ion implanted bulk Si [9-11] as well as for SOI [12-14]. Success in obtaining a fully relaxed, 20nm thick epitaxial Ge layer was demonstrated in ref. [13] through a post-implantation, multiple dry-oxidation process aimed at maintaining the SiGe below its melting point. The implantation-condensation approach negates the requirement for direct epitaxial growth of SiGe, and provides a method for the selective inclusion of SiGe in a complex process flow.

In this paper we present experimental results from a simplified (compared to the work reported in [13]) two step wet oxidation of Ge-implanted SOI and also describe a semi-empirical, model of the process. The higher thermal budgets used in this work subject samples to

temperatures in which high content Ge layers would normally experience melt. This is in general undesirable, resulting in local agglomeration of germanium [15]. However, using transmission electron microscopy we do not observe significant degradation for a sample subjected to a high thermal treatment. This work has relevance to applications which would benefit from high-Ge content, selective SiGe formation to a depth of tens of nanometers. For applications requiring thicker films, the process we describe can provide the high-Ge content seed layer for Ge growth. A similar approach may also provide a suitable seed layer for heterogeneous growth of III-V materials such as GaAs, as described in references [13] and [15].

II. EXPERIMENTAL METHODS

Samples of single crystal 220 nm (SOI) with a 2000 nm Buried-OXide (BOX) were implanted with Ge^+ ions to a fluence of $5x10^{16}$ cm^{-2} and at an energy of 33 keV. Following implantation, thermal oxidation was performed in a tube furnace in a wet O_2 ambient. The samples were initially oxidized at 870℃ for 70 minutes (primary oxidation) and then oxidized again (secondary oxidation) at either 900℃, 1000℃, or 1080℃ with the secondary oxidation being performed incrementally in time on multiple samples in order to examine the formation kinetics of the oxide and the SiGe layer. Samples were oxidized from 15 to 150 minutes in 15 minute increments at 900°C; 10 to 80 minutes in 10 minute increments at 1000°C and 5 to 35 minutes in 5 minute increments at 1080°C. The furnace was calibrated by oxidizing unimplanted, low doped reference Si samples simultaneously with our Ge-implanted samples followed by comparison with the Deal-Grove oxidation model [16]. The primary 870°C oxidation was introduced after our preliminary work indicated that direct high temperature oxidation of the Ge-implanted SOI resulted in majority evaporation of the Ge before any formed oxide layer could act as a diffusion barrier. This is consistent with the work reported in ref. [13]. We note that

minority dose loss occurs during the primary oxidation, which we have quantified and report in the results section of this work. The fabrication process is summarized schematically in Fig. 1.

The fabricated films were analysed using Rutherford Backscattering Spectroscopy (RBS) performed at the 1.7 MV Tandetron Accelerator Facility at Western University. RBS is ideally suited for the extraction of concentration profiles of dissimilar materials from multiple samples, albeit producing results with relatively modest resolution. The probe was a 1.5 MeV He^+ ion beam incident at 7° to the normal of the sample surface with a Si charged particle detector mounted at 170°, with an average counts per sample approximately 27,000. The RBS spectra were analyzed using simulation software SIMNRA (SIMulation of Nuclear Reaction Analysis) [17] in order to determine the composition and thickness of both the oxide and SiGe layers. The system under study is amenable to RBS analysis due to the high Ge content and the significant difference in mass between Ge and Si. We estimate the uncertainties in Ge concentration, Ge layer thickness and SiO_2 thickness obtained through RBS analysis and fitting to be on the order of 5%. The grown oxide thicknesses were independently measured optically. The tool used was a Woollam M-2000 automated angle spectroscopic ellipsometer. This allowed confidence in the extracted profiles obtained from RBS by reducing the number of variables in the SIMNRA simulation.

In order to facilitate Raman Spectroscopy of a subset of the prepared samples, optical excitation was provided by the 325nm line of a He:Cd laser and the scattered light was collected, confocally using a Thorlabs LMU-40x NUV objective lens with a numerical aperture, NA = 0.5, dispersed using a Horiba LabRAM HR Evolution spectrometer and detected with a thermoelectrically cooled Charge-Coupled Device (CCD) camera. We noted that for excitation at longer wavelengths, i.e. at 488nm, the Raman scattering spectra was entirely dominated by the

main Si-Si optical phonon peak (~520cm^{-1}), presumably from the unconsumed thin underlying Si layer. For 488nm, the relative optical penetration depths in bulk silicon and germanium are 569nm and 19nm, respectively, whereas at 325nm, this is ~10nm, for both silicon and germanium. The dramatic increase in the Ge-Ge and Si-Ge scattering peaks (and relative suppression of the Si-Si substrate scattering) we observe for 325nm excitation therefore implies an upper limit on the condensed SiGeOI layer thickness of ~20nm for the samples probed, which we will show is consistent with the RBS analysis.

Transmission electron microscopy (TEM) was performed on a representative sample as a means to assess the crystallinity of the SiGe layer and to provide a verification of the Ge profile in the structures. Scanning-transmission electron microscopy (STEM) and energy dispersive X-ray spectroscopy (EDS) analysis was also performed on the same sample. The electron microscopy and analysis was performed using a JEOL JEM-2010F Field Emission Electron Microscope equipped with an Oxford Instruments EDS analyzer. The sample was exposed to an electron beam accelerating voltage of 200 kV. Elemental maps for Ge, O and Si were obtained (only the Ge profile is shown for clarity). The profile of Ge was obtained using INCAEnergy EDS software, and was plotted together with the STEM images to confirm the location of the Ge. No attempt was made to quantify the Ge concentration using the EDS, and as such the profiles only provide the relative depth distribution of the Ge in the grown oxide and the SiGe layer. TEM (STEM) EDS line scans were obtained with a 1 nm probe diameter.

III. MODEL DESCRIPTION

Modeling of the implantation-condensation process was performed using the commercially available SENTAURUS Technology Computer Aided Design (TCAD) platform provided by Synopsys® [18]. The nature of the model is semi-empirical, however, we show that

the fits to the experimental data yield important insights into the underlying processes at work. The model can be described using three parameters: (1) a segregation coefficient; (2) an enhanced Ge diffusion coefficient (both 1 and 2 are used to model the incorporation of Ge into the oxide as well as the profile of the Ge in the SiGe-On-Insulator layer) and (3) a modified linear rate constant describing the thermal oxidation.

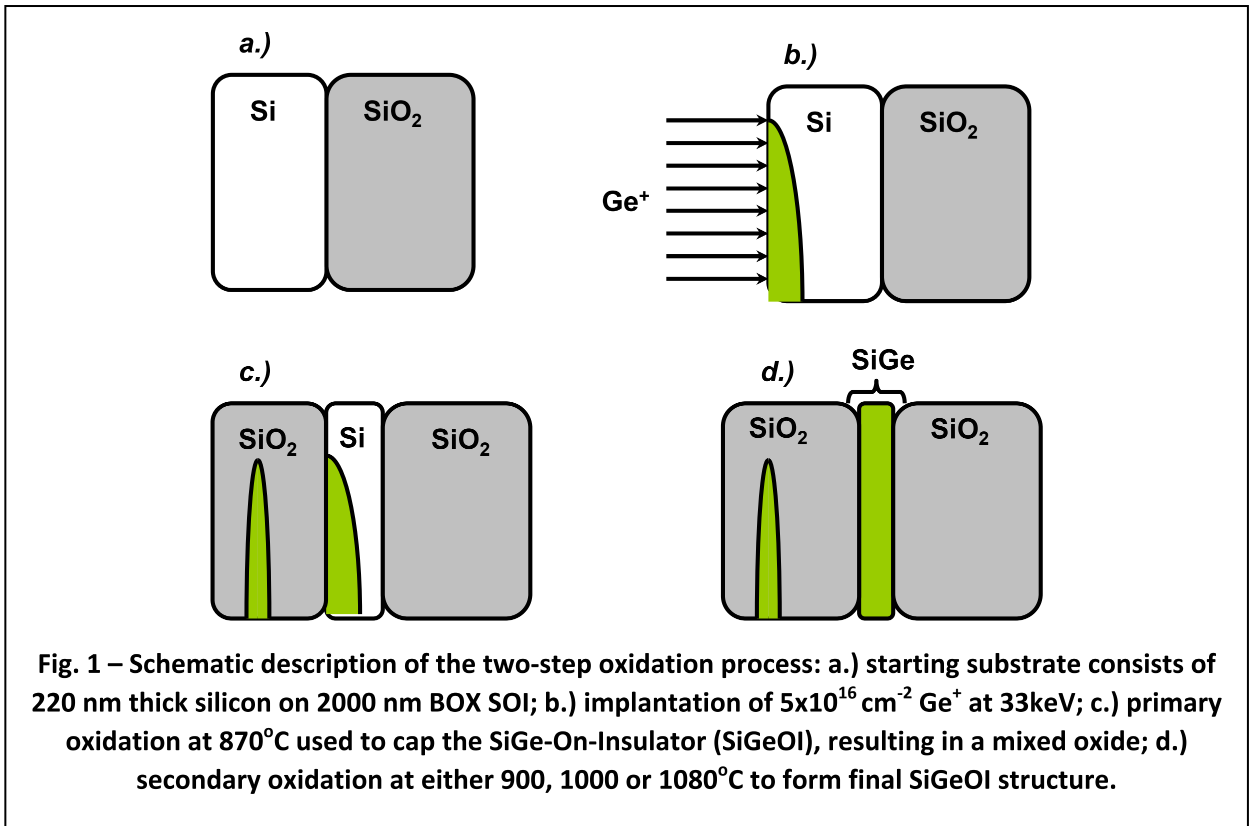

Fig. 1 – Schematic description of the two-step oxidation process: a.) starting substrate consists of 220 nm thick silicon on 2000 nm BOX SOI; b.) implantation of $5x10^{16}$ cm^{-2} Ge^{+} at 33keV; c.) primary oxidation at 870°C used to cap the SiGe-On-Insulator (SiGeOI), resulting in a mixed oxide; d.) secondary oxidation at either 900, 1000 or 1080°C to form final SiGeOI structure.

.

It has been established previously that the presence of Ge enhances the rate of thermal SiO_2 growth [19-22], although Ge should only affect the linear rate constant (as described by the Deal-Grove model [16]) since this is determined by the reaction rate at the growth interface. The presence of Ge should not affect the parabolic rate constant since that is determined by the diffusivity of the oxidizing species through the oxide given that the oxide grown is

predominantly SiO_2. We thus modeled the oxidation using a linear rate constant that was a function of temperature only. Fig. 2 shows the values of the linear rate constant used in simulation of our experimental data, compared with the constant used to describe the oxidation of low-doped, (100) Si. The activation energy for our enhanced linear rate constant (deduced from the Arrhenius relationship) is 1.52 eV, consistent with the predictive modeling by Rabie et al.[23].

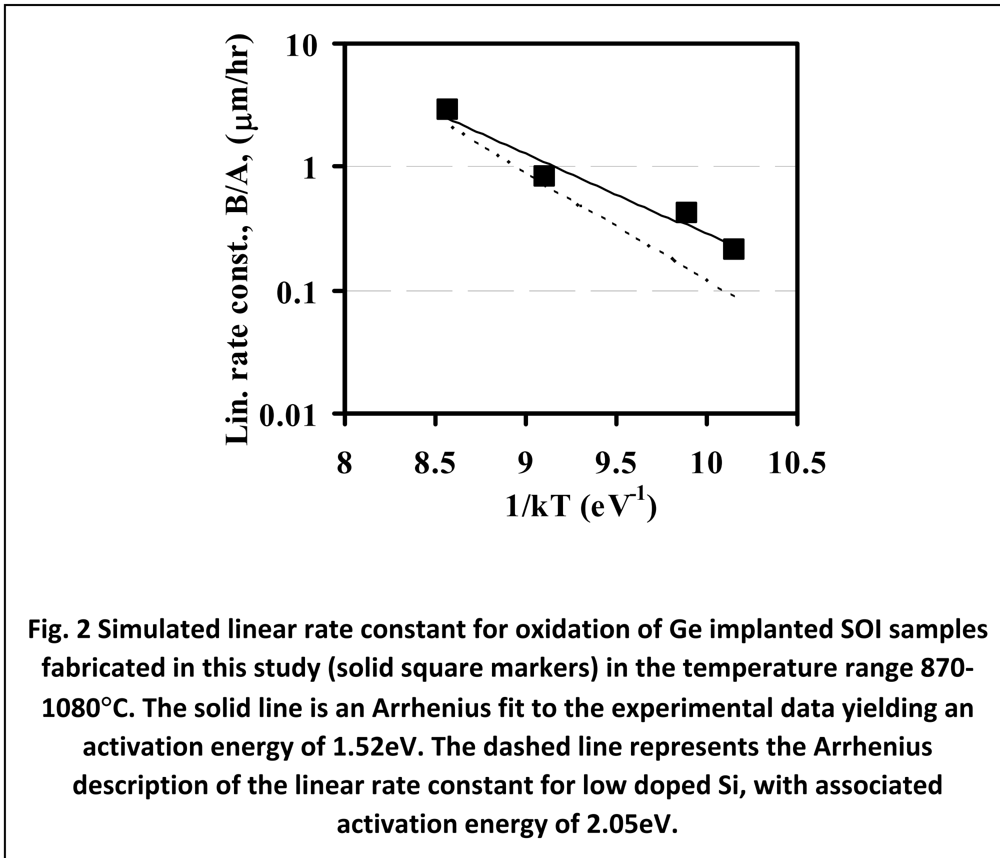

Fig. 2 Simulated linear rate constant for oxidation of Ge implanted SOI samples fabricated in this study (solid square markers) in the temperature range 870-1080°C. The solid line is an Arrhenius fit to the experimental data yielding an activation energy of 1.52eV. The dashed line represents the Arrhenius description of the linear rate constant for low doped Si, with associated activation energy of 2.05eV.

The most important aspect in modeling and deriving a physical understanding of the experimental measurements is the simulation of the Ge pile-up in the remaining SiGe-On-Insulator (SiGeOI) layer after thermal oxidation. In this respect, the Ge segregation coefficient (i.e. the ratio of Ge in the SiGe to that in the oxide at the SiGe/SiO_2 interface) is only important insofar as it determines the total dose of Ge in the oxide and the SiGeOI layer. Several authors

have modeled Ge pile-up by assuming a rejection of Ge from SiO_2 into the Si: effectively an infinite segregation coefficient [see, e.g., Ref. 24]. Others have used a segregation coefficient that is a function of the Ge fraction [18]. Neither of these approaches accounts for the observed formation of mixed oxides under certain experimental conditions (see Ref. [25] and references therein). In our experimental data (for example see Fig. 6 and Fig.11 in section IV) we observe a

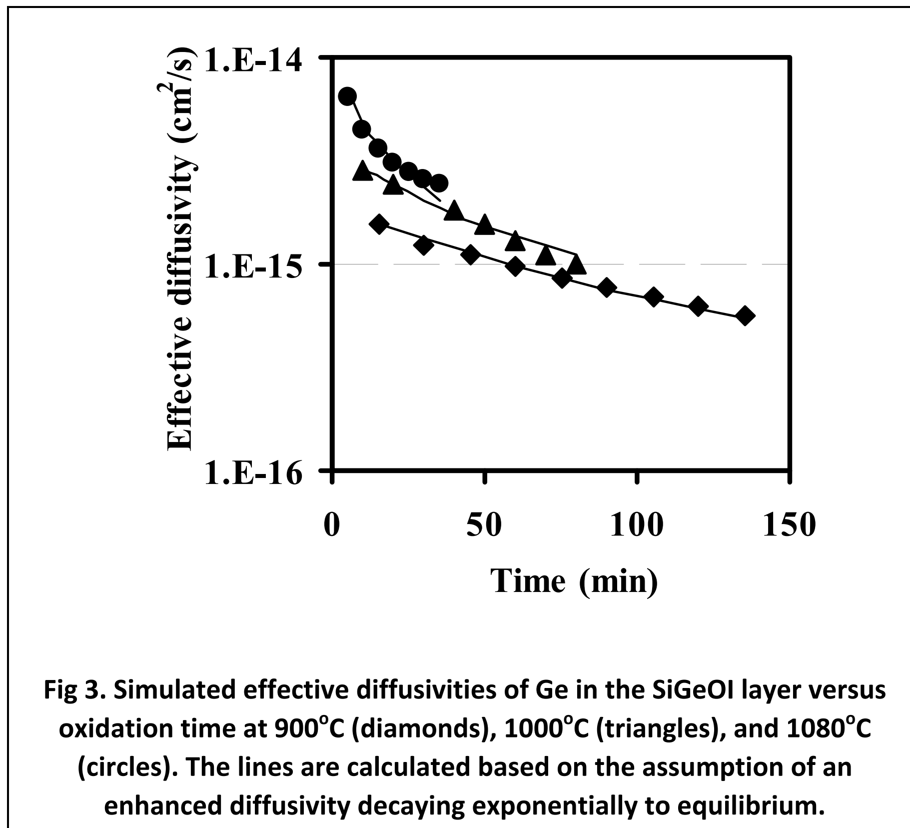

Fig 3. Simulated effective diffusivities of Ge in the SiGeOI layer versus oxidation time at 900°C (diamonds), 1000°C (triangles), and 1080°C (circles). The lines are calculated based on the assumption of an enhanced diffusivity decaying exponentially to equilibrium.

complex pattern whereby during oxidation at 870°C there is an initial oxide layer with no Ge content, followed by the incorporation of Ge in a thin layer, followed by rejection of Ge from the oxide at all subsequent times (and at all higher temperatures). To simulate this pattern, we follow an empirical approach in modeling the incorporation of Ge into the oxide. Specifically, we use the segregation model incorporated in SENTARUS as an ON/OFF 'switch' for the incorporation of Ge in the growing oxide. With segregation ON, we use a constant segregation coefficient =

1000. This is sufficient to exclude all Ge from the growing oxide. There was no requirement to make the segregation coefficient dependent on Ge concentration or temperature. With segregation OFF, we still used a segregation boundary condition but with a segregation coefficient = 1. This ON/OFF switch was used only to describe the experimental results obtained for the primary 870°C oxidation. For all higher, secondary oxidations, which take place following the capping 870°C oxidation, the segregation coefficient was set to ON with a value of 1000. The use of the segregation switch in this purely empirical portion of the model ironically allows us to conclude that segregation is not the dominant mechanism responsible for the incorporation of Ge in the growing oxide. This conclusion is supported through detailed discussion in section IV.

To simulate the Ge profile in the SiGeOI layer at different times and temperatures we used the effective interdiffusivity of Si and Ge as a fitting parameter. The peak concentration of Ge at the growth interface is almost entirely determined by the bulk diffusion behavior [18] whereas the details of the flux of Ge across the growth interface plays only a minor role, primarily in determining the dose of Ge left in the SiGeOI layer. The effective Ge diffusivity at each oxidation temperature, needed to obtain an acceptable fit, is shown in Fig. 3. The lines are fits to the experimental data assuming that the instantaneous diffusivity decays exponentially from an initial value that is significantly higher than equilibrium. While there are differences in previous work regarding the effective interdiffusivity of Si and Ge (see Ref. [26] and references therein) the values in Fig. 3 are seen to correspond to diffusion enhancements on the order of 10^3, 10, and 1 for anneals at 900°, 1000°, and 1080°, respectively. The time constants for the decay in the diffusion enhancement are 41, 21, and 3.4 minutes, respectively.

Assuming an equilibrium diffusivity, D = 310 exp-(4.65/kT) [18], this behavior is fully consistent with Transient Enhanced Diffusion (TED) due to the increased defect density caused by the Ge+ implantation. Most often, TED is associated with residual end-of-range (EOR) defects following amorphizing ion implantation. It is generally assumed that such defects do not play a significant role in enhanced diffusion on the time-scales of our experiment because dissolution of such defects is assumed to take place in a matter of a few seconds at such elevated temperatures [27]. However, recent work on the impact of amorphizing implantation on the performance of solar cells has suggested that extended thermal budgets, used both in solar fabrication and in this work, are not sufficient to remove clustered defects even for anneal temperatures >950°C and duration of >10 minutes [28]. An alternative (and perhaps more convincing) explanation for our observation of enhanced diffusion is the phenomenon of concentration dependent diffusion. For example, ref. [29] describes an experimental study of Ge diffusion in $Si_{1-x}Ge_x$ with *x* ranging from 0 to 0.5. The activation energy for diffusion decreased from 4.7eV to 3.2eV across this range, a result of increased diffusion via a vacancy mechanism with increasing Ge content. Our simulated values of diffusivity (Fig. 3) are consistent with the values obtained in ref [29] while the steep gradient of Ge in our SiGe layer (and its temporal evolution) may explain the simulated decrease in Ge diffusivity with time. The diffusion of Ge in our samples is complex and a study of the detailed kinetics is beyond the scope of this work. We note though that there is no doubt that an enhancement of the (apparent) effective diffusivity of the Ge exists on a timescale that decreases with increasing temperature.

IV. RESULTS AND DISCUSSION

i.) As-implanted profile and that following the primary 870°C oxidation

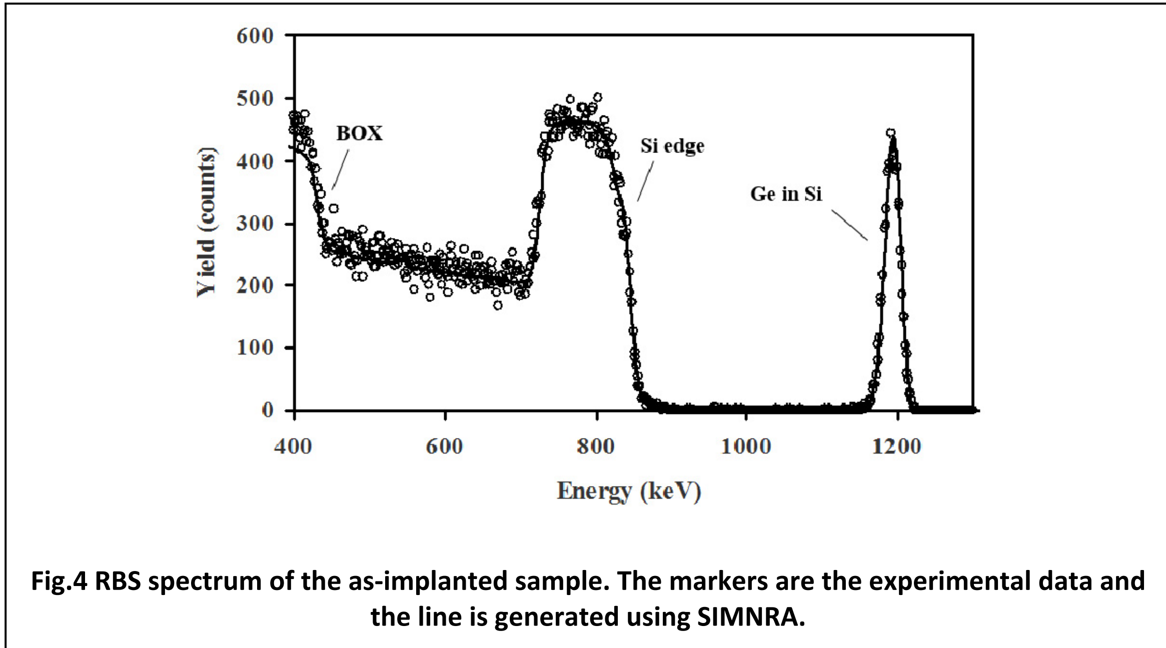

Fig.4 RBS spectrum of the as-implanted sample. The markers are the experimental data and the line is generated using SIMNRA.

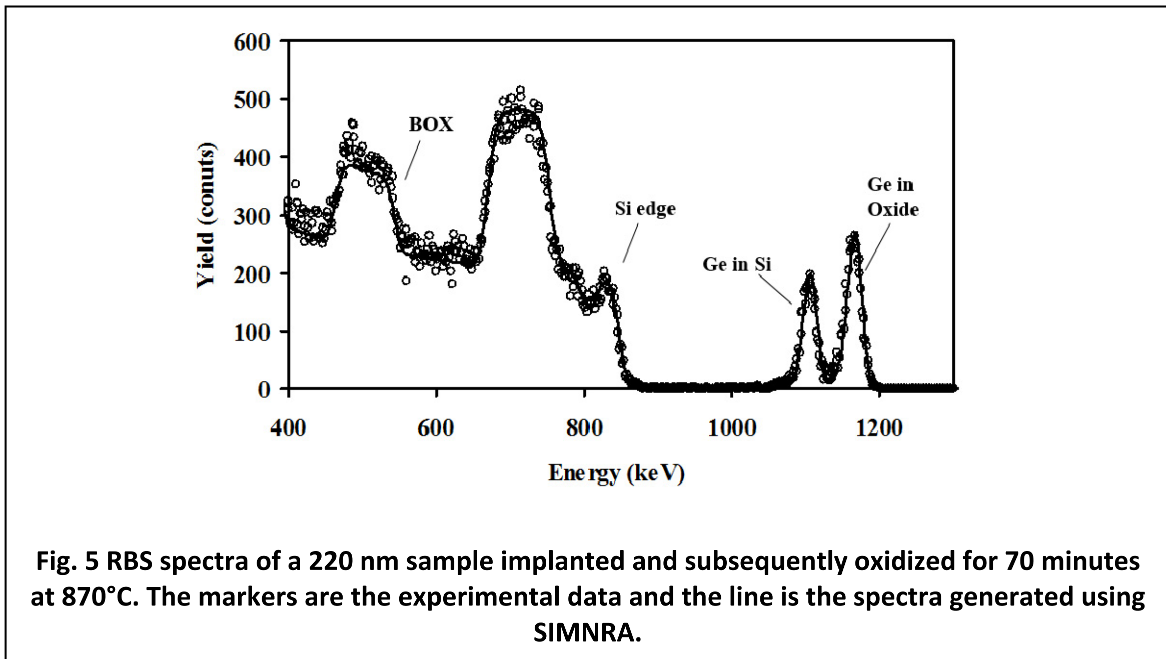

Fig. 5 RBS spectra of a 220 nm sample implanted and subsequently oxidized for 70 minutes at 870°C. The markers are the experimental data and the line is the spectra generated using SIMNRA.

Figs. 4 and 5 show the as-acquired RBS spectra and the simulated profile generated using SIMNRA for an as-implanted sample and a sample after the primary 70 minute oxidation at 870°C. The agreement of the fitted curves with the experimental data is typical of all of those

obtained in this study and thus these serve as representative examples. The experimentally determined as-implanted fluence is 4.8×10^{16} cm^{-2}, (i.e. 4% lower than the nominal implanted fluence of $5x10^{16}cm^{-2}$), likely reflecting a combination of implantation fluence calibration, measurement uncertainty and sample sputtering during the implantation process. The two Ge peaks in Fig. 5 show the incorporation of Ge into the growing oxide layer, and the retention of Ge in the SiGeOI layer. The total retained Ge following the 870°C oxidation is 4.7×10^{16} cm^{-2}, suggesting an approximate further 3% Ge loss during the primary oxidation step, due to Ge evaporation in the early stages of the process. Of the total retained Ge dose, post- 870°C oxidation, approximately 60% was incorporated into the oxide.

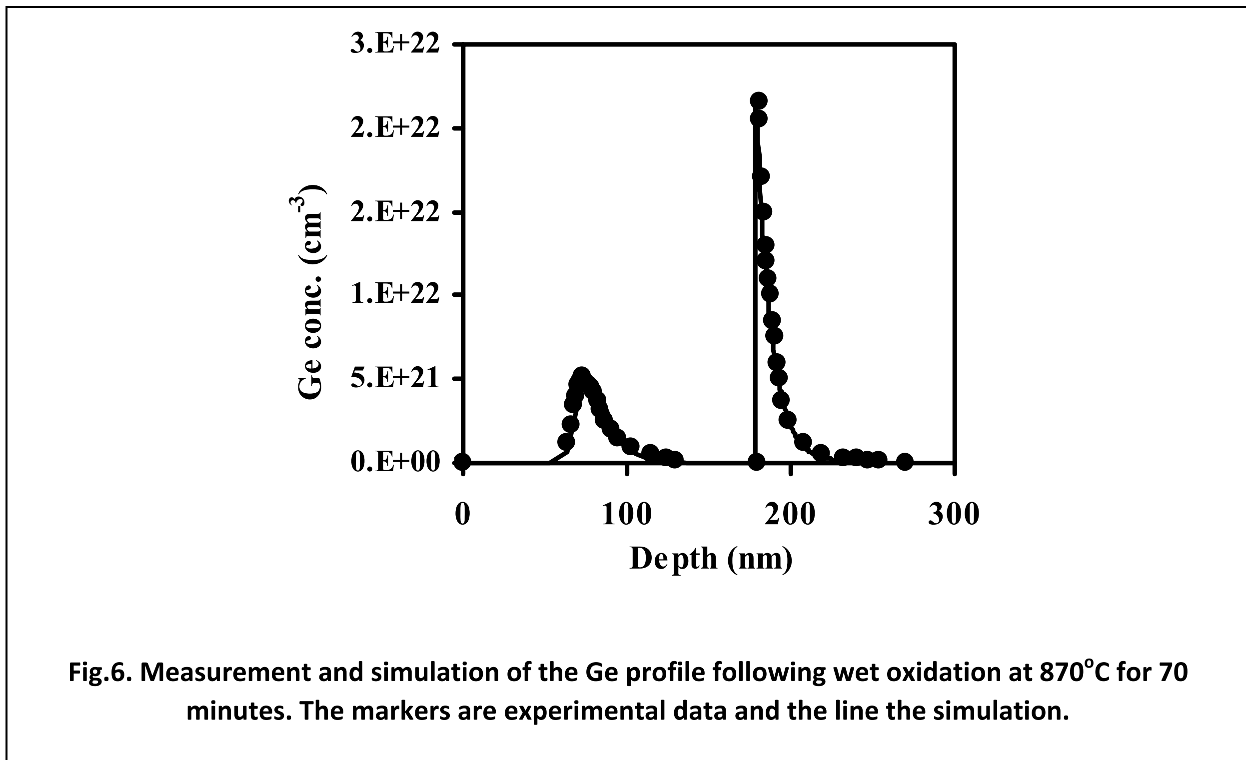

Fig.6. Measurement and simulation of the Ge profile following wet oxidation at 870°C for 70 minutes. The markers are experimental data and the line the simulation.

Fig.6 shows the profile of Ge for the 870°C oxidized sample determined by fitting the RBS data, while the solid line represents simulated results obtained from the TCAD modeling

described in section III. Using the segregation ‘switch’ we found that Ge was rejected from the growing oxide for the first 27 minutes of oxidation time at 870°C (segregation switch set to ON); incorporated into the oxide for 6 minutes (segregation switch set to OFF); then rejected from the oxide for the remaining 36 minutes (segregation switch returned to ON). The quality of the fit to our experimental data, shown in Fig.6, obtained with this binary empirical simulation leads to two important conclusions. First, the fit to the Ge profile in the oxide with no segregation at all during the narrow time window when Ge is incorporated in the growing oxide supports the thesis that segregation alone is not the dominant process determining Ge incorporation into the growing oxide. While we note that our ON/OFF segregation switch can be useful as an empirical tool to fit the data, not only is segregation consideration not predictive of the conditions for Ge incorporation/rejection but it is actually physically incorrect in that when Ge is incorporated into the oxide it is incorporated at the same concentration as the Ge present at the surface. Second, if we momentarily ignore the top 65 nm of the sample (SiO_2) where there is no Ge in the oxide, the behavior of the Ge is more consistent with the predictions of the kinetic model of Rabie et al. [22]. That model is based on the assumption that Ge and Si are both oxidized simultaneously at similar rates (although Si oxidation is moderately faster) but that a portion of the Ge is then replaced in the oxide through a replacement reaction that removes GeO_2 and forms SiO_2 in its place. The amount of Ge in the oxide is determined by the rate of this reaction, the instantaneous oxidation rate, and the availability of Si at the growth interface, which is in turn controlled by the diffusion behavior of Si in the SiGe layer. The incorporation of Ge is therefore better explained by a rapid oxidation rate compared with the diffusion of Si to the interface and then drops as the oxide thickness increases slowing the arrival rate of oxidant at the interface compared with that of Si. This explanation also provides insight regarding the initial 65 nm Ge-free oxide for the

870°C oxidation. The first 27 minutes of oxidation occur during a period that includes the solid phase regrowth of the implantation amorphised SiGeOI layer, and subsequently a period in which residual defects persist. In the highly defective layer, both the reaction rate and the diffusivity of Si to the surface would be significantly higher than for the recrystallized layer [30] so that the replacement reaction would be sufficient to replace any Ge in the oxide. Similar enhanced diffusivity is evidenced by the data in Fig. 3 for a time period consistent with 27 minutes, i.e. the period of time in which excess defects are present in the SiGeOI layer for the 900°C oxidation.

ii.) Oxide growth and Ge profiles for 900, 1000, 1080°C secondary oxidations

As previously explained, it was deemed preferable to initially oxidize all samples at 870°C for 70 minutes in order to cap the SiGe layer and thus prevent majority evaporation of Ge during the condensation process. Even so, we note that this primary oxidation results in ~60% of the

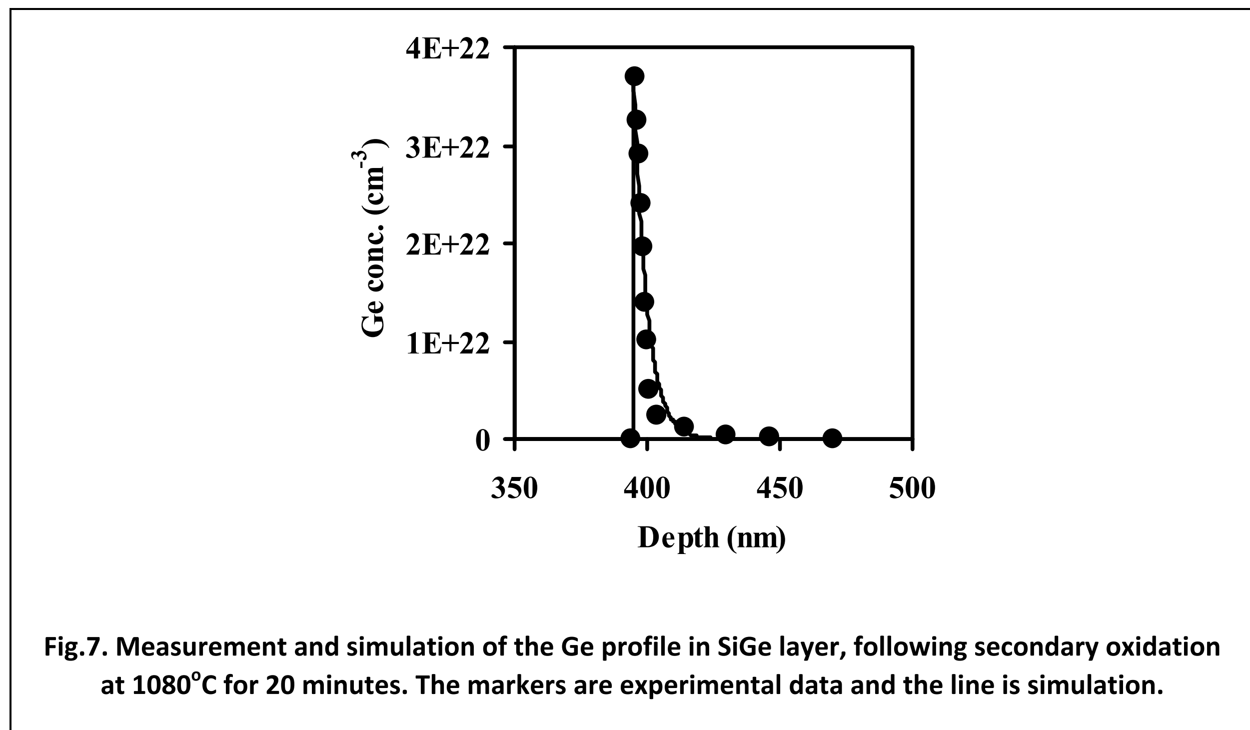

Fig.7. Measurement and simulation of the Ge profile in SiGe layer, following secondary oxidation at 1080°C for 20 minutes. The markers are experimental data and the line is simulation.

implanted Ge being incorporated into the grown oxide in a somewhat complex process for which detailed, quantitative explanation is beyond the physically meaningful capabilities of the TCAD model used. We anticipate that future experimental and theoretical work will permit an optimized primary oxidation in which suitable capping is achieved without a relatively large fraction of Ge-oxide incorporation.

The Ge profile measured following the primary oxidation becomes the starting condition for all subsequent secondary oxidations. In Fig. 7 we show the experimentally determined profile of Ge in the SiGeOI layer of the sample which was subjected to a secondary oxidation at 1080°C for 20 minutes. The Ge is piled-up at the SiGe/SiO_2 interface, here located at 395nm from the sample surface (i.e. the grown oxide has a thickness of 395nm).

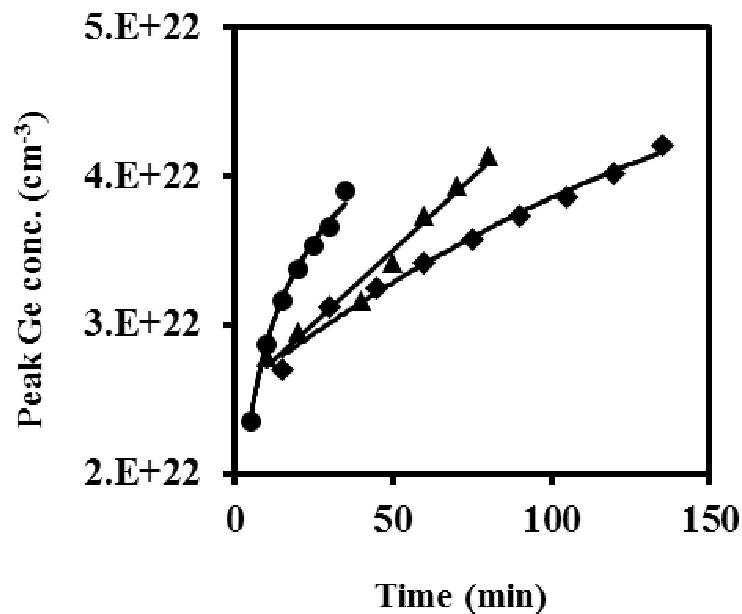

Fig. 8 Peak concentration of Ge at the oxide/SiGeOI interface as a function of secondary oxidation time for 900°C (diamonds), 1000°C (triangles), and 1080°C (circles). The lines are guides to the eye. The model described in section III replicated the experimental values by using the effective Ge diffusivity values summarised in Fig.3.

The solid line is the simulated profile obtained using the model described in section III, albeit with the segregation switch ON during the secondary oxidation, thus enforcing a complete rejection of the Ge from the oxide. We note that Ge remains present in the oxide with the same profile as that shown in Fig.6 (following primary oxidation) although it is not shown in Fig.7 as to highlight the agreement of the experimental and simulated profiles. Such agreement is representative of that obtained for all secondary oxidations indicating that the model (which in this case is determined by the fitted oxidation rate and Ge diffusivity) is physically representative of the processes which determine the Ge concentration profile, and thus offer a means for predictive determination.

Fig. 8 shows the peak Ge concentration at the SiO_2/SiGe interface as a function of temperature and secondary oxidation time, while Fig. 9 shows the simulated oxide thickness and experimental values as a function of temperature and oxidation time.

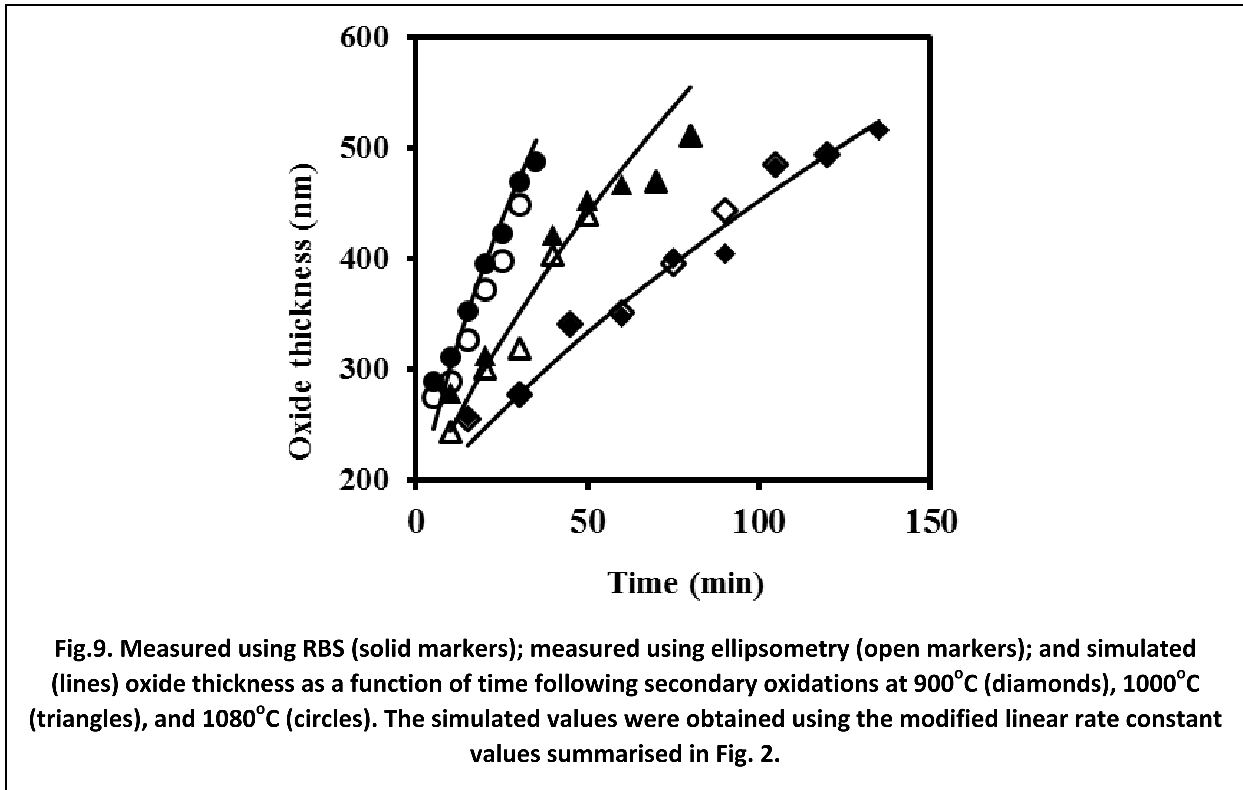

Fig.9. Measured using RBS (solid markers); measured using ellipsometry (open markers); and simulated (lines) oxide thickness as a function of time following secondary oxidations at 900°C (diamonds), 1000°C (triangles), and 1080°C (circles). The simulated values were obtained using the modified linear rate constant values summarised in Fig. 2.

iii.) Transmission Electron Microscopy (TEM) and Scanning Transmission Electron Microscopy (STEM) images

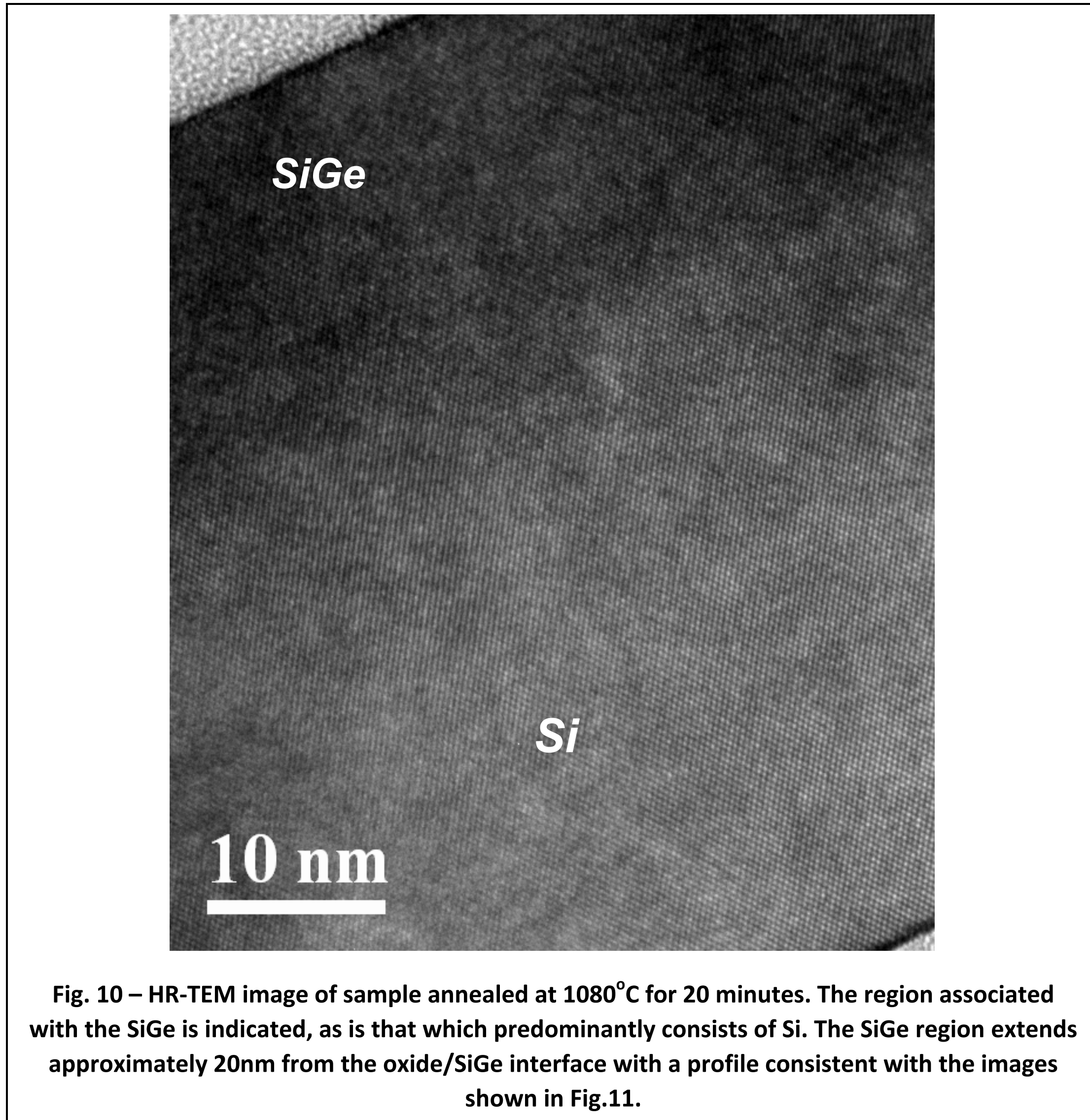

Fig. 10 – HR-TEM image of sample annealed at 1080°C for 20 minutes. The region associated with the SiGe is indicated, as is that which predominantly consists of Si. The SiGe region extends approximately 20nm from the oxide/SiGe interface with a profile consistent with the images shown in Fig.11.

Fig. 10 shows a representative High Resolution-TEM (HR-TEM) image; in this case for the SiGe layer formed after annealing at 1080°C for 20 minutes where the peak concentration of Ge is approximately 75 at- %. The image confirms the crystalline nature of the sample indicating the successful seeding of the SiGe layer from the underlying Si not amorphised by the Ge^+ implantation. While we make no attempt in this work to quantify residual defects (such as

dislocations) we can confirm that the volume probed by us was predominantly defect free, and as such the image is representative of the quality of this sample. Fig. 11 shows STEM images of the same sample in both low and moderate magnification. The nature of the STEM measurement emphasizes contrast for species of different mass. Further, the species giving rise to the contrast can be determined using EDS. In Fig.11 we show EDS spectra for Ge superimposed onto the STEM images thus providing an unambiguous confirmation that the contrast in the STEM is due to the incorporated Ge.

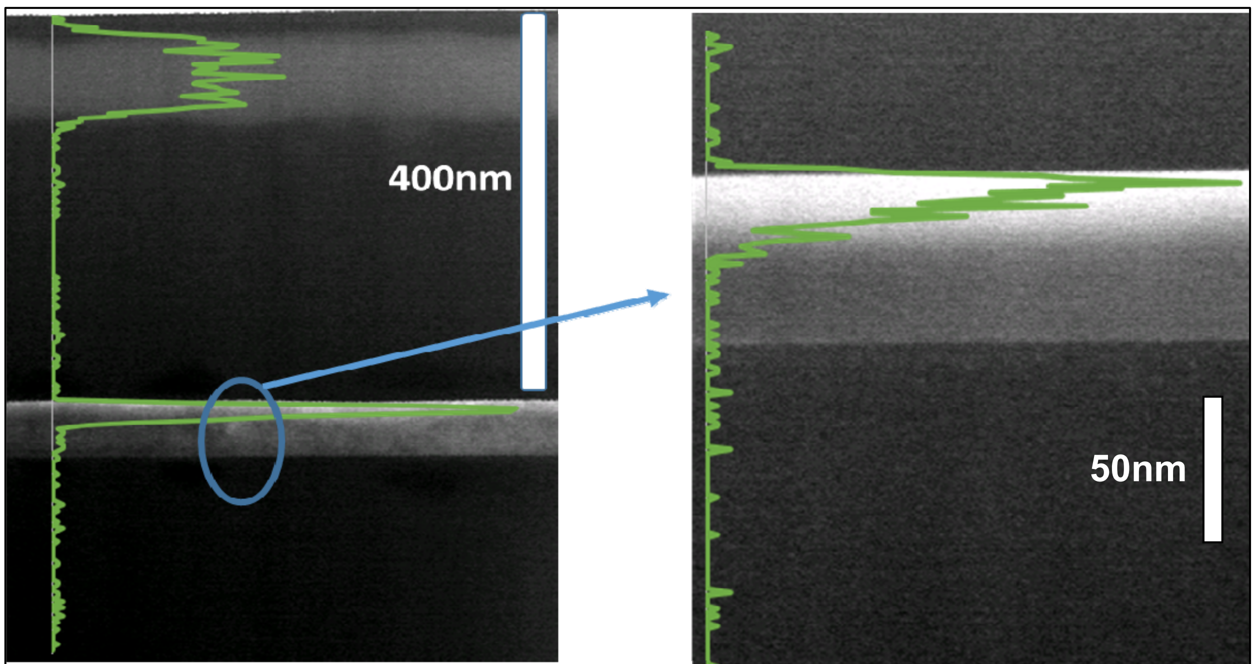

Fig.11 – (left) STEM image of sample oxidized at 1080°C for 20 minutes with Ge EDS spectra superimposed (green solid line) indicating a mixed oxide band and Ge profile in SiGe layer; (right) higher magnification STEM image of same sample indicating SiGe layer only, again with Ge profile superimposed. The Ge EDS profile indicates the relative depth distribution only with no attempt to provide a quantification of the Ge concentration.

In this way, we are able to compare the STEM images with profiles obtained via RBS to confirm the presence of the mixed Ge/Si band. In the case of STEM the band is measured to have a width ~85nm in the grown oxide at a depth of ~30nm from the sample surface. Further, the profile of

the Ge within the SiGe layer itself is seen to be consistent with the profile shown in Fig. 7. We note that for the lower magnification image in Fig 11 the Ge contained in the oxide shows signs of non-uniformity. The high concentration of Ge in these samples gives rise to an oxidation temperature that would increase in excess of the compound melt temperature for the 1080°C oxidations. This has been shown previously to result in non-uniform agglomeration of condensed Ge [15]. No such agglomeration within the SiGe is seen in the samples shown in Fig.11. Future work will be aimed at confirming this effect for samples prepared using the implantation-condensation process. We also plan a comprehensive exploration of the concentration and impact of implantation induced defects using the TEM technique.

iv.) Raman Spectroscopy

Fig. 12 shows the evolution of the Raman scattering spectra with thermal budget for samples receiving secondary oxidation anneals at 900°C, for 135 minutes, 1000°C for 60 minutes and 1080°C for 35minutes. Raman measurements were performed after removal of the top (grown) oxide via etching in dilute HF acid. In order to enable direct comparison of the Si-Si alloy scattering in the SiGe layer with the the Ge-Ge scattering peak, contributions from the underlying (pure) silicon layers, owing to their different frequency, were subtracted from the total scattering spectra, after fitting these with a Lorentzian line-shape function. All of the samples exhibit peaks associated with the Ge-Ge (~300cm^{-1}), Si-Si (~500cm^{-1}) and SiGe (~400cm^{-1}) scattering with the peak positions varying during the oxidation. In SiGe alloys the scattering peak positions are known to be sensitive to both strain and composition, which makes it difficult to extract reliable values for either in a system in which both may be changing.

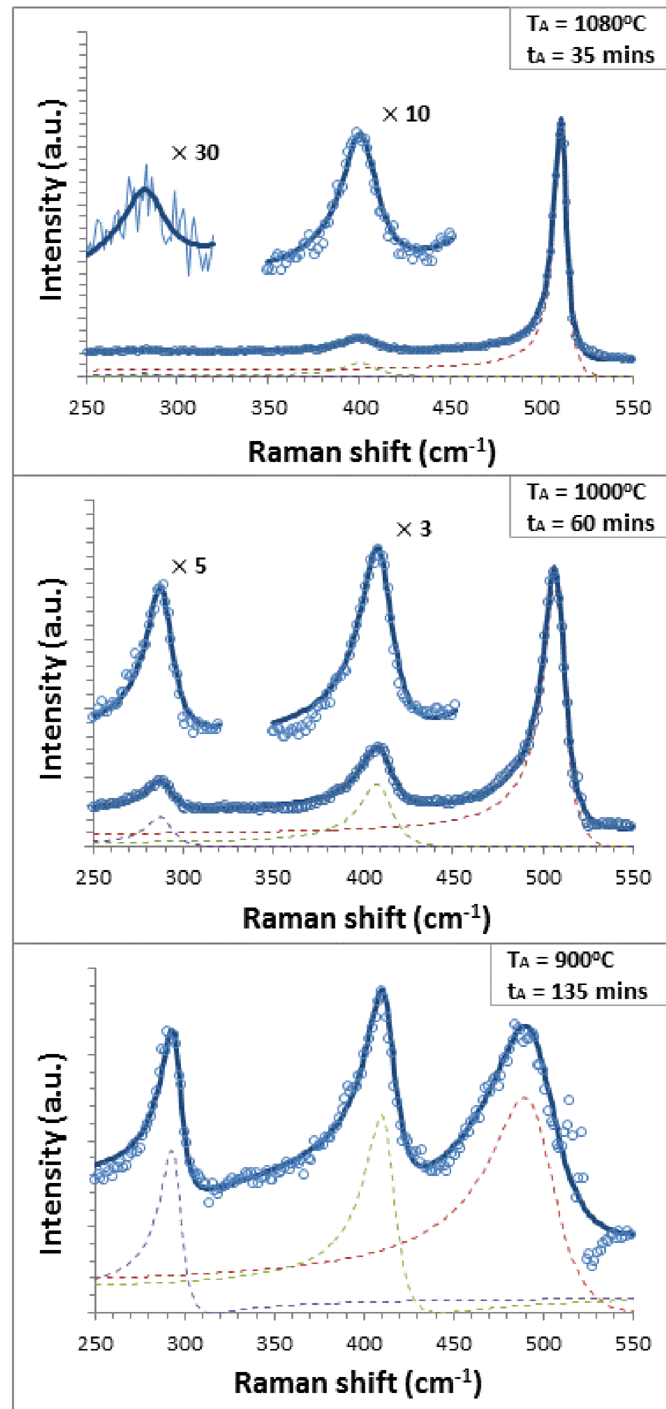

Fig. 12 Evolution of the scattering spectra from the SiGe layer as a function of thermal budget during oxidation annealing. The contribution from the Si substrate has been subtracted to enable direct comparison of the Si-Si alloy scattering in the SiGe layer with the Ge-Ge scattering peak. Integrated peak intensities and frequencies were determined from the fitted lines, which are asymmetric (Fano) line-shape functions, after reference [32].

However, one can use the relative scattering intensities as a means to determine the compositional fraction because, in a simplified treatment of the SiGe layer as a purely random mixture of Si and Ge atoms, the probability of finding either Si-Si or Ge-Ge vibrating pairs as a function of the Ge composition, is simply proportional to the relative numbers of corresponding bond types [31]. If the Raman scattering intensity for either of these modes is then assumed to be proportional to the number of these vibrating pairs within the layer, then the ratio of scattering intensities should vary according to:

$$\frac{I_{Ge-Ge}}{I_{Si-Si}}(x) = \frac{x^2}{(1-x)^2} \qquad (1).$$

This function reveals the Ge concentration in the SiGe layers to be ~44 at-% at 900°C, ~26 at-% at 1000°C and ~12 at-% at 1080°C. This result appears to be in disagreement with the RBS measurements which indicate (for example) that the peak concentration for a sample annealed at 900°C for 135minutes, is close to 95 at-%. We believe that the consistently lower Ge composition determined using single wavelength excitation (UV) Raman scattering is a result of the narrow width of the SiGe layer and a consequent optical probing of the tail of the Ge distribution. That is to say, although the two techniques appear to be reporting very different Ge compositional fractions, we are confident that this is only the result of probing different regions of the highly non-uniform (that is, non-uniform in depth) thin SiGe layer.

Having determined the Ge compositional fraction at a specific depth using the ratio of integrated Raman peaks, we examined the peak positions of the three main scattering modes; Si-Si, Si-Ge and Ge-Ge in order to determine whether and to what degree there is any inherent strain in the SiGe layer. The precise scattering frequency of these peaks depends on both layer composition and strain, ε according to the following empirical relations [32]:

$$\omega(x,\varepsilon)_{Si-Si} = 520.5 - 70x + b_{Si}\varepsilon \quad (2)$$

$$\omega(x,\varepsilon)_{Si-Ge} = 400.1 + 24.5x - 4.5x^2 - 33.5x^2 + b_{SiGe}\varepsilon \quad (3)$$

$$\omega(x,\varepsilon)_{Ge-Ge} = 282.5 + 19x + b_{Ge}\varepsilon \quad (4)$$

where the coefficients b_m are phenomenological parameters that depend on the elastic constants of the specific materials; Si, SiGe and Ge. Taking the coefficients determined previously by Pezzoli et al [34] to be: b_{Si} = -730cm^{-1}, b_{SiGe} = -570cm^{-1} and b_{Ge} = -450cm^{-1} we find a highly consistent agreement for the strain for all three modes. Fig. 13 is the graphical representation of Eqs. (2)-(4) illustrating the Raman shift with Ge alloy composition and strain for the three main optical phonon modes in SiGe. The measured peak positions and Ge alloy compositions we have determined here indicate that where the Ge fraction is highest, (i.e. for our measurement taken from the sample annealed at 900°C for 135 minutes) there exists a significant compressive strain ε ~1%. As the thermal budget is increased, the combined intermixing of the Si with the SiGe layer (or out diffusion of Ge from that region) acts to reduce this compressive strain so that for annealing at 1000°C for 60 minutes, ε is reduced to ~0.7% and for the sample annealed at 1080°C for 35 minutes, it is almost completely relaxed (within experimental error). These increased values of compressive strain with Ge composition in ultra-thin SiGeOI layers
are in very good agreement with previous work on similar ultra-thin SiGe layers [35], although contrary to the implantation-condensation samples of reference [13].

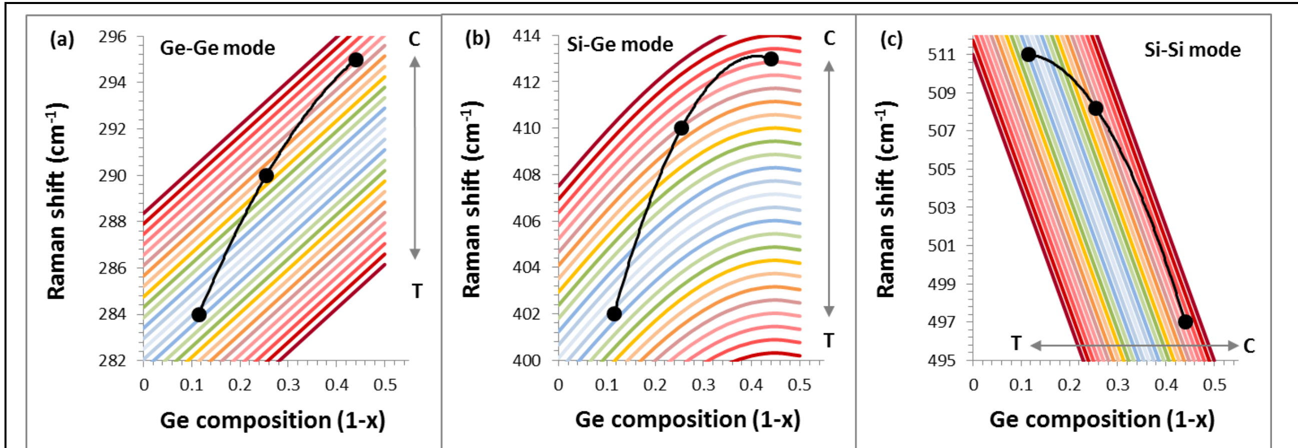

Fig. 13 - Predicted Raman shift for (a) Ge-Ge, (b) Si-Ge and (c) Si-Si alloy modes as a function of Ge concentration (1-x) for various values of strain, either tensile (T) or compressive (C) in the range 1.3% to -1.3% (0.1% increments). The points determined for the samples studied here (connected by lines to guide the eye) show a strongly correlated behaviour for all three modes; a significant (~1%) compressive strain in the sample with the highest Ge content, ~44 at-% (annealed at 900°C for 135 minutes) is gradually relaxed as the Ge fraction diminishes with thermal budget during annealing.

v.) Future work

The data in Fig.7 demonstrate that a maximum peak concentration approaching 95 at-% has been obtained which suggests a technique capable of producing high Ge content SiGeOI. While the ratio of Si to Ge can be mediated via the annealing conditions, the thickness of the SiGe layer is limited to tens of nm's and future work will investigate processes using higher energy implants and optimized initial capping oxides with the aim to increase layer thickness. We also plan improvements in modeling of our experimental data. In order to construct a completely predictive, physically-based model, we refer to Py et al. [36] and Uematsu [37] who have demonstrated the necessity of solving a full system of equations taking into account the behavior of point defects and conservation of lattice site density as in the model of Hasanuzzaman et al. [38 and 39]. For the concentrations of Ge used here and in other similar experiments, ignoring the conservation of lattice site density can lead to the unphysical result of a greater number of

substitutional atoms than lattice points, for example. Further, we did not attempt in this study to model the diffusion behavior of Ge in the oxide or to experimentally determine the state of Ge in the oxide to confirm the mixed oxide expected if the Rabie model [20] is correct. We thus concede then that a full model of the process described here would require the use of kinetic oxidation simulation, the full interdiffusion of Si and Ge, including the conservation of lattice site density, and the diffusion of Ge in the oxide. However, we do assert that the preliminary model presented does shed light on the dominant physical processes of the implantation-condensation process, and in a limited sense the model provides predictive capabilities. Comprehensive characterization is planned in support of the descriptive model. Of primary importance is the need for structure imaging and residual defect characterization, atomic force microscopy for the determination of surface roughness and a broader study of induced strain evolution. Such work will allow us to compare the implantation-condensation process with condensation using epitaxial growth as a starting point.

V. CONCLUSION

We have demonstrated a germanium implantation-condensation technique using Ge-implanted SOI utilizing a two-step wet oxidation process. Our experimental matrix is preceded by an initial oxidation at 870°C to minimize out-gassing of Ge, followed by a higher temperature oxidation at either 900°C, 1000°C or 1080°C for incremental periods of time in order to examine the formation of the oxide and Ge layer over time. Samples were characterized using RBS analysis to examine the composition and thickness of the oxide and Ge layer and then compared with a semi-empirical model. The dominant fitting parameters in this model are a modified segregation boundary condition and a linear oxidation rate enhancement which are attributed to

the replacement reaction of Ge in oxide with silicon; and an enhanced diffusion coefficient for Ge which is consistent with transient enhanced diffusion. TEM and STEM analysis of a representative sample shows that the SiGe is relatively uniform and defect free, while EDS profile data is consistent with the RBS anaylsis of the same sample. Raman spectroscopy shows that significant compressive stress can be induced in the SiGe layers at levels consistent with previous condensation studies in which epitaxially grown SiGe provided the primary structure.

ACKNOWLEDGEMENTS

We gratefully acknowledge funding from the Natural Sciences and Engineering Research Council of Canada (NSERC) in support of this work. RA acknowledges stipend support via the NSERC CREATE training program, SiEPIC. We thank Doris Stevanovic of the Centre for Emerging Device Technologies, McMaster University for assistance with sample preparation and Dr. Lyudmila Goncharova of Western University for assistance with RBS analysis. We acknowledge useful discussions with Dr Simon Ruffell. We thank Dr Zhilin Peng for preparation of the TEM samples and Dr Carmen Andrei for help in TEM and STEM measurements.

REFERENCES

[1] B. Vincent, J. Damlencourt, Y. Morand, A. Pouydebasque, C. Le Royer, L. Clavelier, N. Dechoux, P. Rivallin, T. Nguyem, S. Critoloveanu, Y. Campidelli, D. Rouchon, M. Mermoux, S. Deloenibus, D. Bensahel, T. Billon, *Mat. Sci. in Semicond. Process.* **11,** 205 (2008)

[2] J. Osmond, G. Isella, D. Chrastina, R. Kaufmann, M. Acciarri, H. Kanel, Appl. Phys. Lett. **94** 201106 (2009)

[3] T. Loh, H. Nguyen, C. Trung, A.Trigg, G. Lo, N. Balasubrmanian, D. Kwong, S. Tripathy, Appl. Phys. Lett. **90**, 092108 (2007)

[4] M. Jutzi, M. Berroth, G. Wohl, M. Oehme, and E. Kasper, IEEE Photon. Technol. Lett. **17**, 1510 (2005)

[5] J. Wang, S. Lee, Appl. Phys. Lett. **11** 696 (2011)

[6] R. E. Camacho-Aguilera, Y. Cai, N. Patel, J. T. Bessette, M. Romagnoli, L. C. Kimerling, and J. Michel, Opt. Express **20**, 11316-11320 (2012)

[7] B. Troia, J. Soler-Penades, A. Z. Khokhar, M. Nedeljkovic, C. Alonso-Ramos, V. M. N. Passaro, and G. Z. Mashanovich, Optics Letters, **41** 610 (2016).

[8] S. Nakahrai, T. Tezuka, N. Sugiyama, Y. Moriyama, S. Takagi, Appl. Phys. Lett. **87**, 3516 (2003)

[9] D. Fathy, O. W. Holland, C. W. White, Appl. Phys. Lett. **51**, 520 (1987)

[10] D. Fathy, O. W. Holland, C. W. White Appl. Phys. Lett. **51**, 1337 (1987)

[11] K. Hossain, L. K. Savage, O. W. Holland, Nuc. Instr. And Meth. in Phys. B **241**, 553 (2005)

[12] D. Choi, B. Luther-Davies, T. Kim, K. Belay, D. Llewellyn, R. G. Elliman., in *the Proceedings of the Conference on Optoelectronic and Microelectronic Materials and Devices,* IEEE, Canberra, Australia, December 12 – 15, 2010, pp. 155-156.

[13] D. Choi, B. Luther-Davies, T. Kim, R. G. Elliman., in *the Proceedings of the IEEE International Conference on Nanotechnology,* Portland, Oregon, USA, August 15 – 18, 2011, pp. 1668-1672.

[14] R. Anthony, and A. P. Knights, in *Journal of Physics: Conference Series*, IOP Publishing, Leeds, United Kingdom, August, 3-8, 2014.

[15] H. J. Oh, K. J. Choi, W. Y. Loh, T. Htoo, S. J. Chua, and B. J. Cho, J. Appl. Phys. **102**, 054306, (2007)

[16] B. E. Deal , A. S. Grove, J. Appl. Phys. 36, 3770 (1965).

[17] M. Mayer, SIMNRA User's Guide, Report IPP 9/113 (Max-Planck-Institute fur Plasmaphysik, Garching, Germany, 1997)

[18] Synopsys User Manuals, *Advanced Calibration for Process Simulation User Guide*, Synopsys (2016).

[19] F.K. LeGoues, R. Rosenberg, T. Nguyen, F. Himpsel, and B.S. Meyerson, J. Appl. Phys. **65**, 1724 (1989).

[20] E.C. Frey, N. Yu, B. Patnaik, N.R. Parikh, M.L. Swanson, and W.K. Chu, J. Appl. Phys. **74**, 4750 (1993).

[21] W.S. Liu, E.W. Lee, M.A. Nicolet, V. Arbet-Engels, K.L. Wang, N.M. Abuhadba, and C.R. Aita, J. Appl. Phys. **71**, 4015 (1992).

[22] J.P. Zhang, P.L.F. Hemment, S.M. Newstead, A.R. Powell, T.E. Whall, and E.H.C. Parker, Thin Solid Films **222**, 141 (1992).

[23] M.A. Rabie, Y.M. Haddara, and J. Carette, J. Appl. Phys. **98**, 074904 (2005).

[24] T. David, A. Benkouider, J.-N. Aqua, M. Cabie, L. Favre, T. Neisius, M. Abbarchi, M. Naffouti, A. Ronda, K. Liu, and I. Berbezier, J. Phys. Chem. C **119**, 24606 (2015).

[25] M.A. Rabie, M.A.Sc. Thesis, McMaster University (2006).

[26] Y. Dong, Y. Lin, S. Li, S. McCoy, and G. Xia, J. Appl. Phys. **111**, 044909 (2012).

[27] C.J. Ortiz, P. Pichler, T. Führer, B. Colombeau and N. E. B. Cowern and A. Claverie, J. Appl. Phys. **96**, 4866 (2004).

[28] F. A.Wolf, A. Martinez-Limia, D. Stichtenoth, and P. Pichler, IEEE Journal of Photovoltaics, **4**, 851 (2014).

[29] N. R. Zangenberg, J. Lundsgaard Hansen, J. Fage-Pedersen, and A. Nylandsted Larsen, Ge Self-Diffusion in Epitaxial $Si_{1-x}Ge_x$ Layers, Phys. Rev. Lett., **87**, 125901 (2001).

[30] F. Strauss, L. Dorrer, T. Geue, J. Stahn, A. Koutsioubas, S. Mattauch, H. Schmidt, Phys. Rev. Lett. **116**, 025901 (2016)

[31] F. Pezzoli, L. Martinelli, E. Grilli, A. Guzzi, S. Sanguinetti, M.Bollani, H. D. Chrastina, G.Isella, H. von Kanel, E. Wintersberger, J. Stangl, and G. Bauer, Mats. Sci. and Eng.B Solid State Materials for Advanced Technology **124-S1**, 127 (2005).

[32] N. Fukata, K. Sato, M. Mitome, Y. Bando, T. Sekiguchi, M. Kirkham, J. I. Hong, Z. L. Wang, R. L. Snyder, ACS Nano, **4**, 3808 (2010).

[33] G. Capellini, M. De Seta, Y. Busby, M. Pea, F. Evangelisti, G. Nicotra, C. Spinella, M. Nardone, and C. Ferrari, J. Appl. Phys., **107**, 063504 (2014).

[34] F. Pezzoli, E. Bonera, E. Grilli, M. Guzzi, S. Sanguinetti, D. Chrastina, G. Isella, H. von Känel, E. Wintersberger, J. Stangl, and G. Bauer, J. Appl. Phys. **103**, 093521 (2008).

[35] T.Tezuka, N. Hirashita, Y. Moriyama, S. Nakaharai, and N. Sugiyama, Applied Phys. Letts., **90**, 181918 (2007)

[36] M. Py, J.P. Barnes, P. Rivallin, A. Pakfar, T. Denneulin, D. Cooper, and J.M. Hartmann, J. Appl. Phys. **110**, 044510 (2011).

[37] M. Uematsu, "Self-diffusion and dopant diffusion in germanium (Ge) and silicon-germanium (SiGe) alloys," in Y. Shiraki and N. Usami (eds.), *Silicon-germanium (SiGe) nanostructures*, pp. 299-337, Woodhead Publishing, Cambridge, UK (2011).

[38] M. Hasanuzzaman and Y.M. Haddara, J. Mater. Sci.: Mater. In Electron. **19**, 569 (2008).

[39] M. Hasanuzzaman, Y.M. Haddara, and A.P. Knights, J. Appl. Phys. **105**, 043504 (2009).

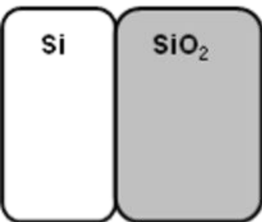
a.)
Si
SiO_2
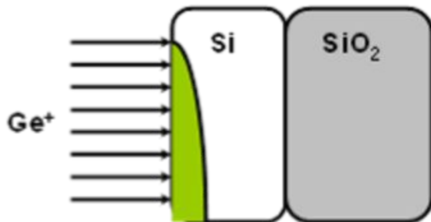
b.)
Ge^+
Si
SiO_2
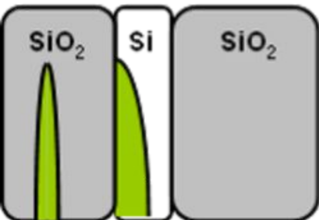
c.)
SiO_2
Si
SiO_2
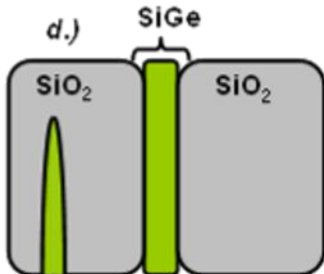
d.)
SiGe
SiO_2
SiO_2

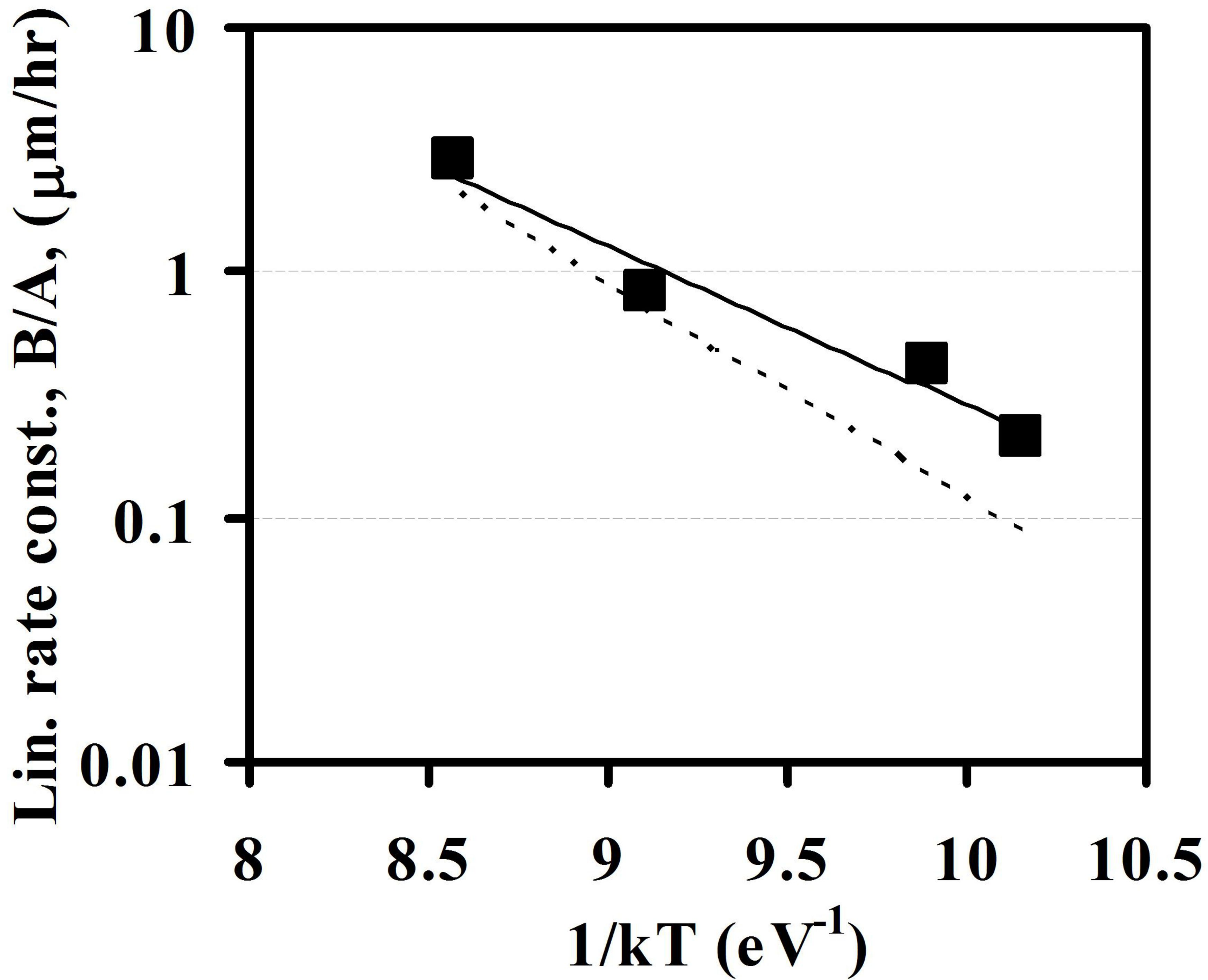

Lin. rate const., B/A, (μm/hr)
10
1
0.1
0.01
8
8.5
9
9.5
10
10.5
1/kT (eV-1)

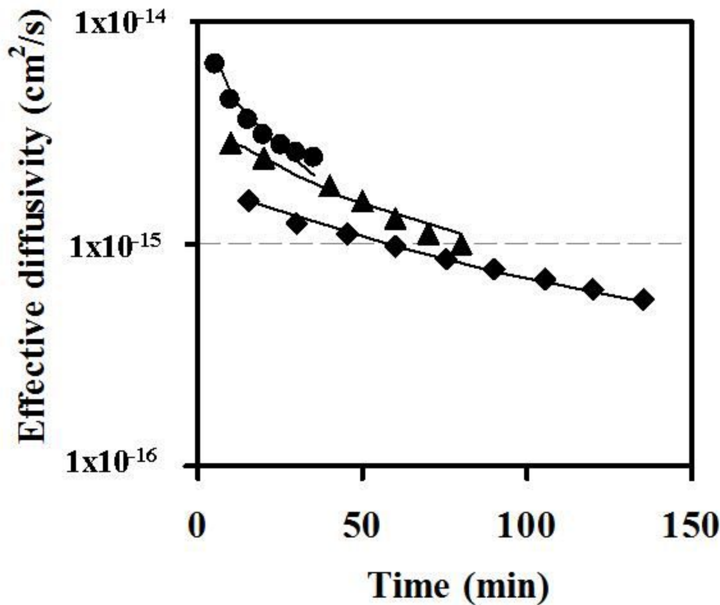

1x10-14
1x10-15
1x10-16
Effective diffusivity (cm2/s)
0
50
100
150
Time (min)

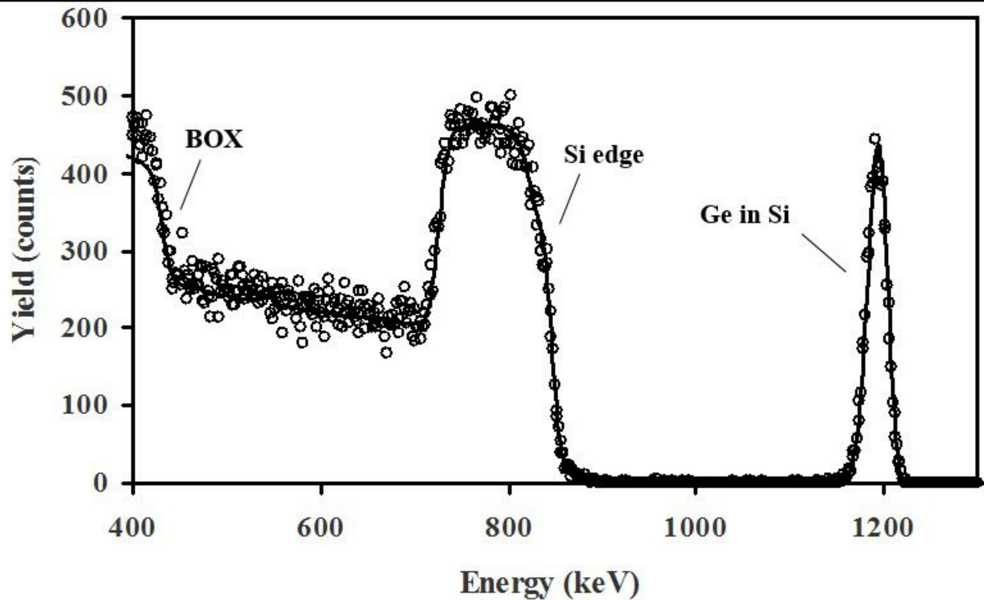

Yield (counts)
Energy (keV)
BOX
Si edge
Ge in Si
600
500
400
300
200
100
0
400
600
800
1000
1200

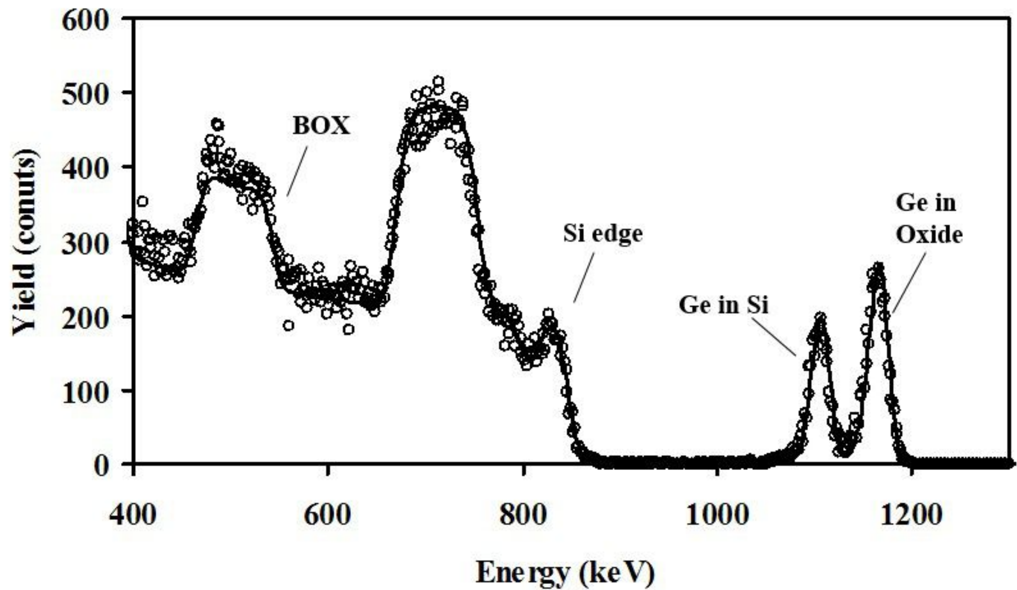

600
500
400
300
200
100
0
400
600
800
1000
1200
Yield (conuts)
Energy (keV)
BOX
Si edge
Ge in Si
Ge in
Oxide

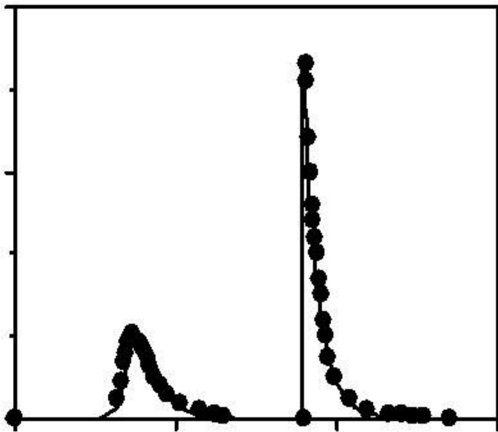

2x10^22
1x10^22
0
Ge conc. (cm^-3)
0
100
200
300
Depth (nm)

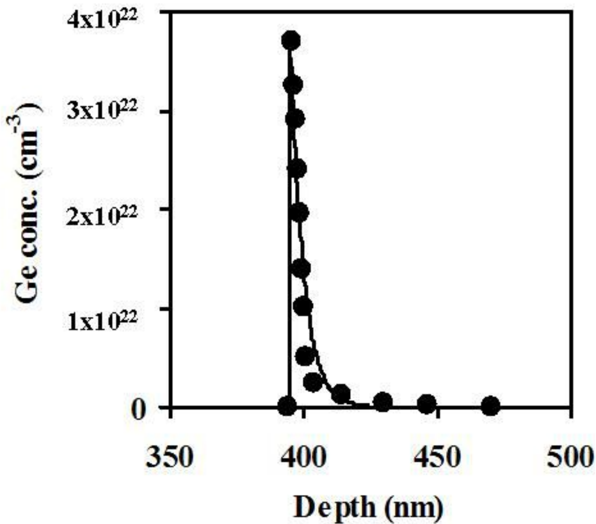
4x10^22
3x10^22
2x10^22
1x10^22
0
Ge conc. (cm^-3)
350
400
450
500
Depth (nm)

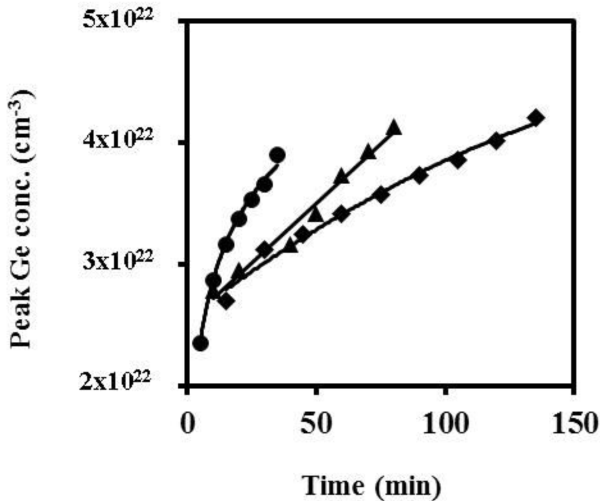

Peak Ge conc. (cm-3)
5x1022
4x1022
3x1022
2x1022
0
50
100
150
Time (min)

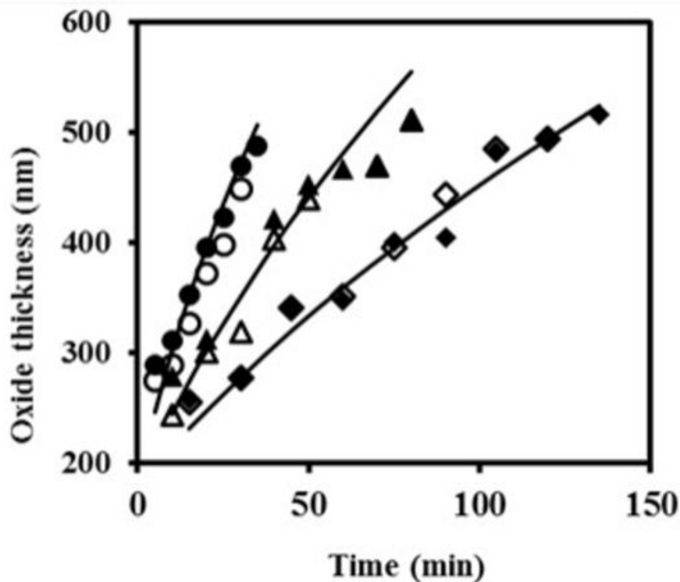
600
500
400
300
200
Oxide thickness (nm)
0
50
100
150
Time (min)

SiGe
Si
10 nm

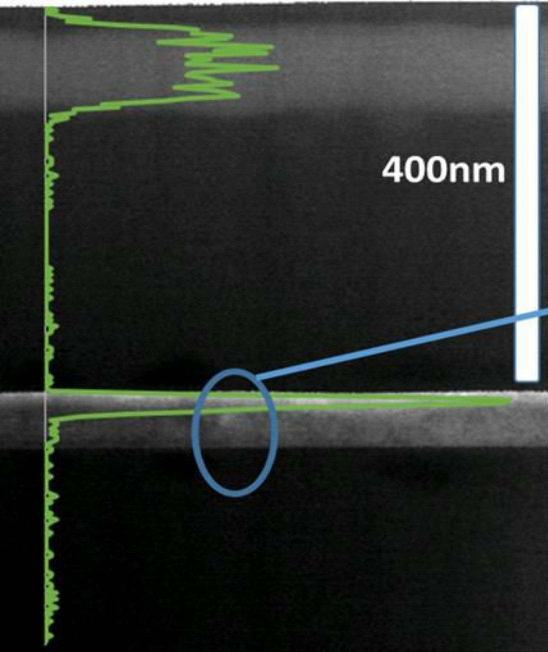
400nm

50nm

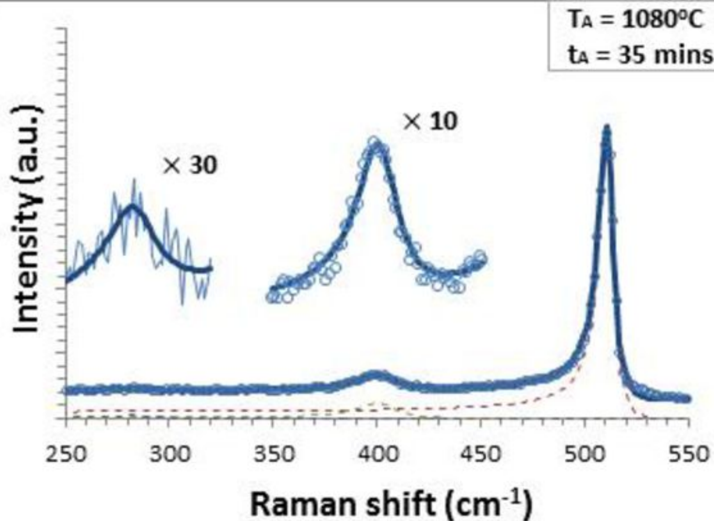

TA = 1080ºC
tA = 35 mins
× 30
× 10
Intensity (a.u.)
250 300 350 400 450 500 550
Raman shift (cm-1)

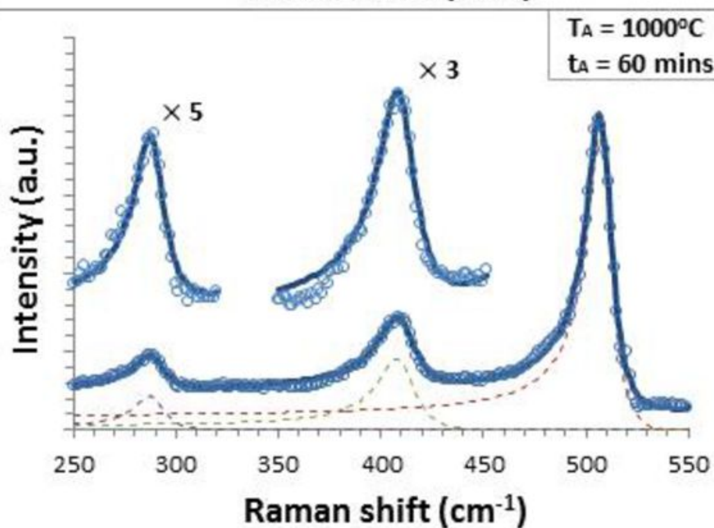

TA = 1000ºC
tA = 60 mins
× 5
× 3
Intensity (a.u.)
250 300 350 400 450 500 550
Raman shift (cm-1)

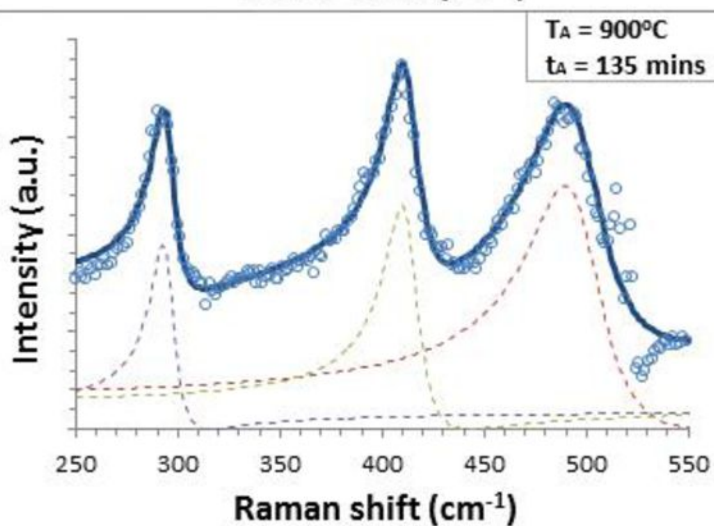

TA = 900ºC
tA = 135 mins
Intensity (a.u.)
250 300 350 400 450 500 550
Raman shift (cm-1)

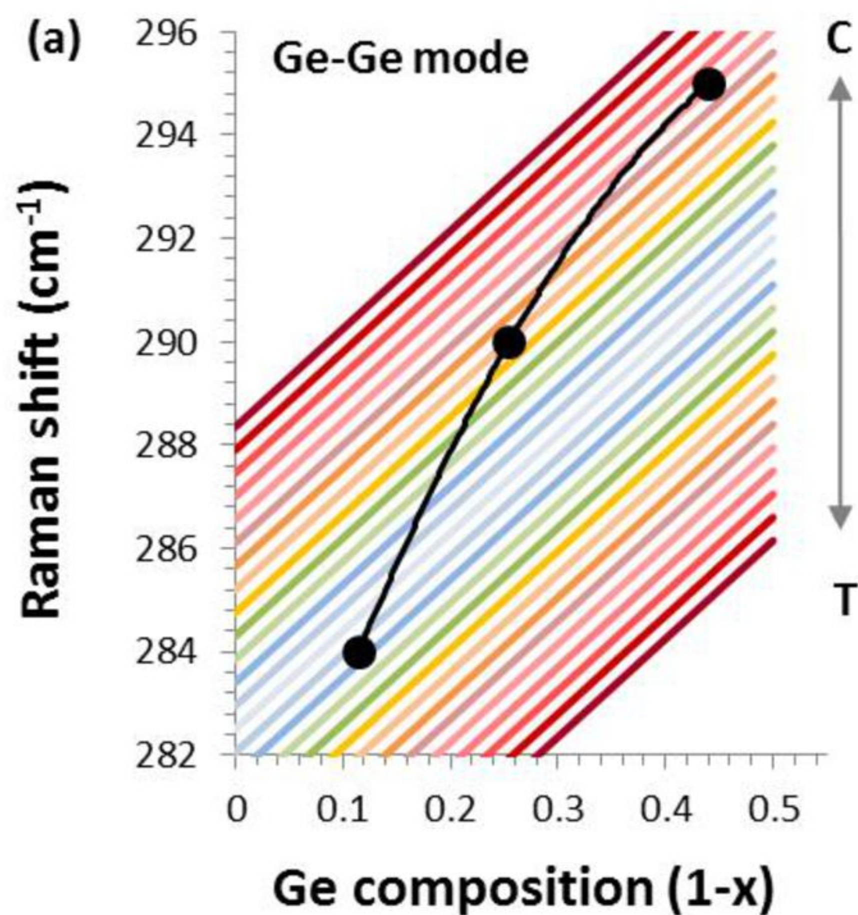
(a)
Ge-Ge mode
C
T
Raman shift (cm^{-1})
296
294
292
290
288
286
284
282
0
0.1
0.2
0.3
0.4
0.5
Ge composition (1-x)

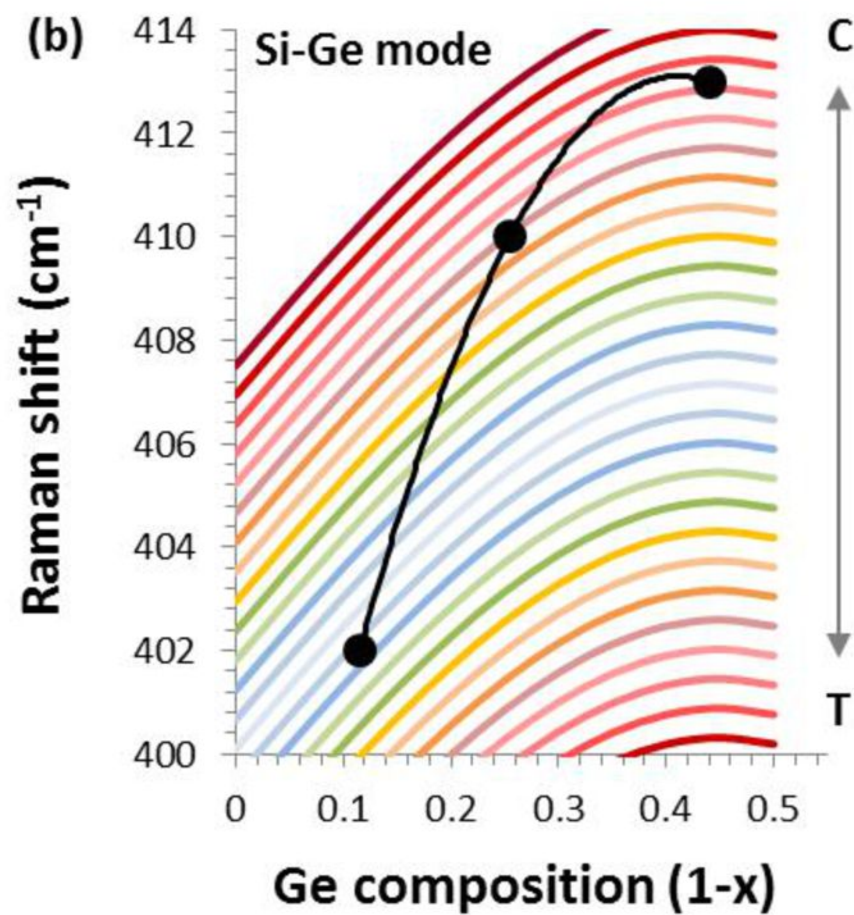
(b)
Si-Ge mode
C
T
Raman shift (cm^{-1})
414
412
410
408
406
404
402
400
0
0.1
0.2
0.3
0.4
0.5
Ge composition (1-x)

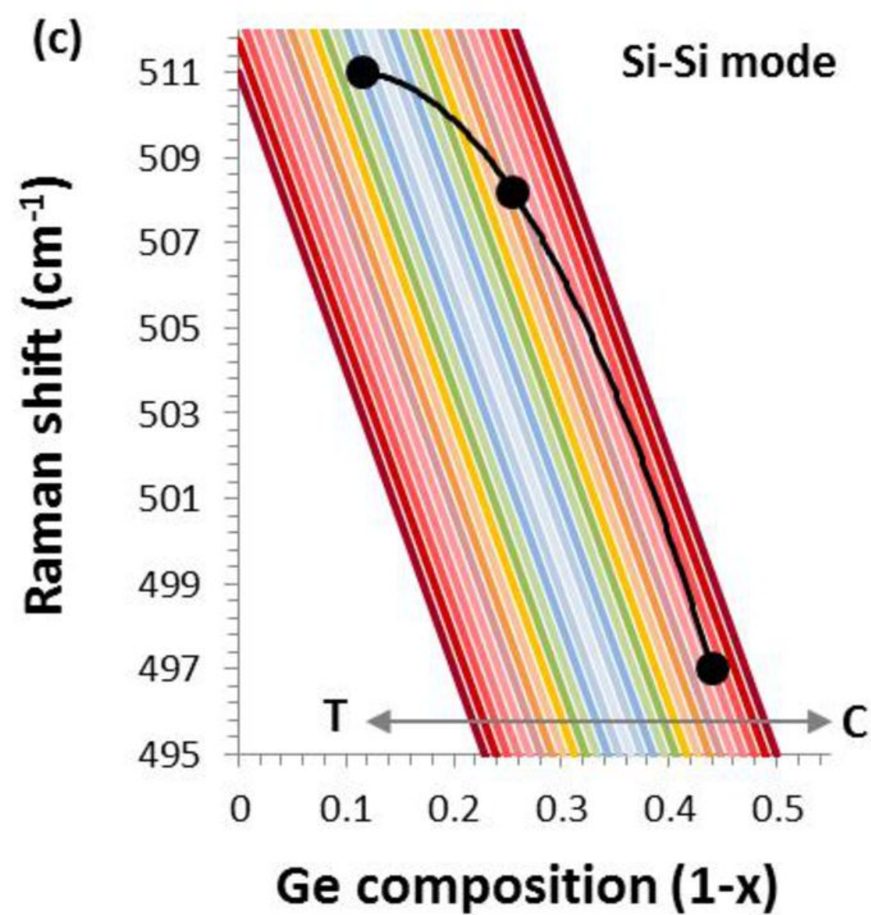
(c)
Si-Si mode
T
C
Raman shift (cm^{-1})
511
509
507
505
503
501
499
497
495
0
0.1
0.2
0.3
0.4
0.5
Ge composition (1-x)